Towards Self-Consistent Tearing Mode Evolution and Micro-Turbulence Interaction in Gyrokinetics

F. Widmer[1,2], E. Poli[2], A. Ishizawa[3],
A. Mishchenko[4], A. Bottino[2], T. Hayward-Schneider[2],

[1]National Institutes of Natural Sciences, Headquarters for Co-Creation Strategy, International Research Collaboration Center (IRCC) Tokyo, Japan
Max Planck Institute for Plasma Physics, [2]Garching, [4]Greifswald,Germany
[3]University of Kyoto, Kyoto, Japan

MAX-PLANCK-INSTITUT
FÜR PLASMAPHYSIK

November 29th-30th, 2023

Magnetic Reconnection in Astrophysics: Solar flares

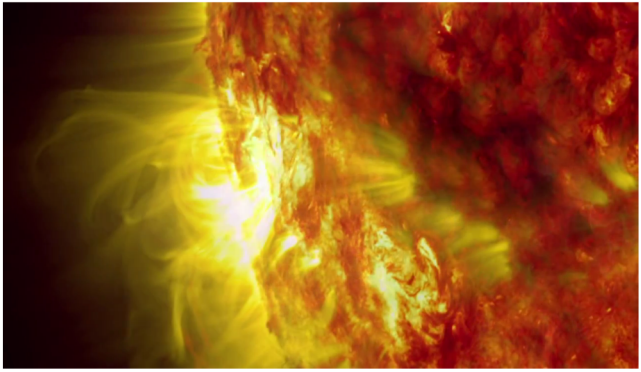

Credits: http://science.nasa.gov

Magnetic Reconnection in Laboratory: Tokamak

Axisymmetric torus-shaped vessel with large magnetic field, moderate plasma pressure and small toroidal current

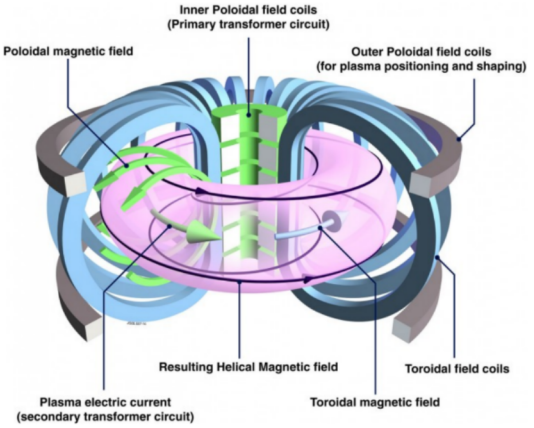

Credits: www.ccfe.ac.uk

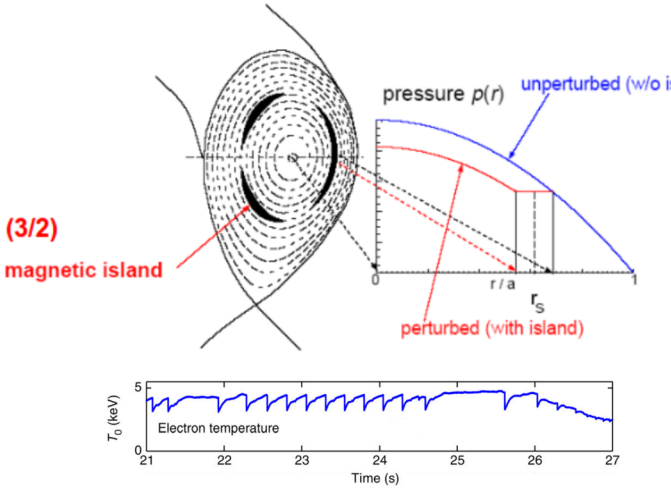

- Multiple reconnection events: Sawteeth, Edge Localized Modes (ELMS), Magnetic islands

Reconnection in Toroidal Geometry: Helical Magnetic Field B^*

- Torodial field created externally. Do not take part in reconnection (strong guide-field)
- Poloidal field do not change sign over the tokamak radius
- The helical magnetic field B^* changes sign across $q = q_s \rightarrow$ possibility to reconnect
- B^* described by the helical flux function Ψ^* obtained integrating $\boldsymbol{B}$

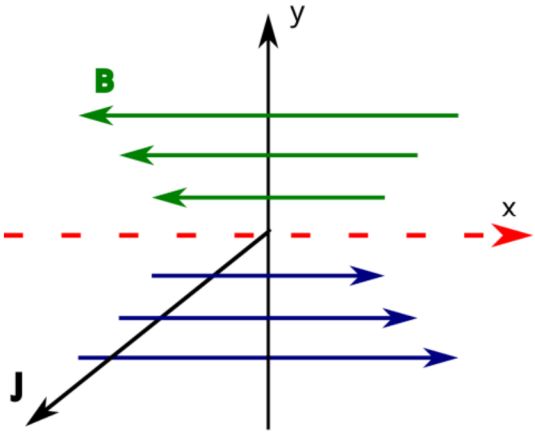

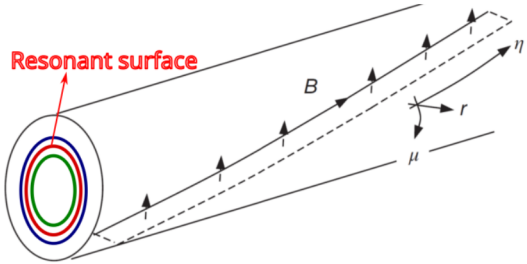

Helical co-ordinate system relative to the field lines on a resonant surface (Zohm 2014)

Tearing Mode in Slab and Cylindrical Geometry

Slab geometry: equilibrium $\boldsymbol{B}$ from CS

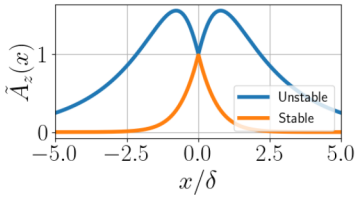

$$\widetilde{A}_z \propto e^{(-k_y|x|)}\left(1+\frac{\tanh(|x/\delta|)}{k_y\delta}\right)$$

- $\partial_x \widetilde{A}_z$ not continuous
- Tearing parameter $\Delta' = \lim_{\epsilon\to 0} \frac{\partial \ln(\tilde{A}_z)}{\partial x}\Big|_{x=-\epsilon}^{x=+\epsilon}$
- $\delta\Delta' = 2\left(\frac{1}{(\delta k_y)} - \delta k_y\right)$

$$\gamma = (\Delta')^{4/5} k_y^{2/5} L_s^{6/5} \tau_A^{-2/5} \tau_R^{-3/5}$$
$$\approx \eta^{3/5} (\Delta')^{4/5} \left(\frac{k_y B_0}{L_s}\right)^{2/5}$$

Cylindrical geometry: $\boldsymbol{B}$ shearing

Helical field B^* prone to tearing

Tearing Equation:

$$\Delta\boldsymbol{\Psi}_1^* - \frac{\mu_0(dj_{0z}/dr)}{B_{0\theta}(r)(1-q(r)n/m)}\boldsymbol{\Psi}_1^* = 0$$
$$\partial_r \boldsymbol{\Psi}^* = -B_{0\mu}^*$$

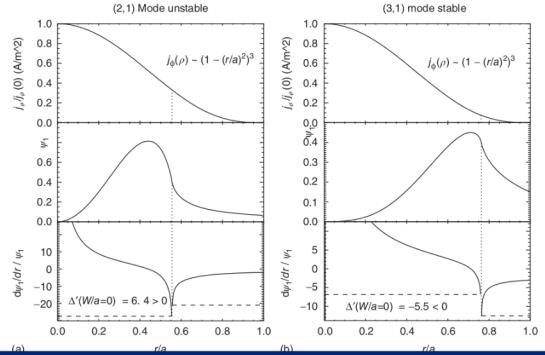

Lagrangian PIC code ORB5

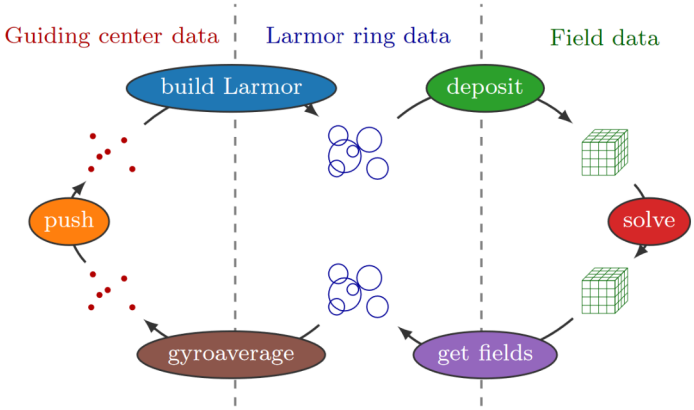

Figure 3: Main stages of an ORB5 time step. The 6-fold scheme differs from the usual PIC 4-fold scheme because of the introduction of the Larmor ring data.

Figure – Main stages of an ORB5 time step. The 6-fold scheme differs from the usual PIC 4-fold scheme because of the introduction of the Larmor ring data. Ohana *et al.* CPC 21

Gyrokinetic Assumptions

Gyrokinetic: average the fast particle gyration to reduce 6D kinetic theory to 5D

Assumptions:

- Time scale separation between collective fluctuations and the fast gyro-motion of a particle in a strongly magnetized plasma.
- Strongly magnetized unperturbed plasma: $\rho_s \nabla(\boldsymbol{B})/\boldsymbol{B} = \rho_s/R \ll 1$
- Removal of the fast cyclotron timescale: $\omega/\omega_c \ll 1$
- Spacial variation of background quantities χ of the order of major radius R: $|\nabla\chi|/|\chi| = \nabla \ln|\chi| \cong 1/R$
- The gyro-radius is much smaller that the device size and much larger than the Debye length: $\rho_s/R \ll 1$ and $\rho \gg \lambda_D$
- The fields fluctuations are allowed to vary on the scale of the gyro-radius only in the direction perpendicular to the field $k_\perp \rho = \epsilon_\perp \cong 1$ and $k_{||}/k_\perp \ll 1$
- $k_\perp \rho_s \approx 1 \rightarrow$ GK relevant to micro-scale perturbations but also to few ρ_i size that characterize MHD modes singularities.
- Perturbations amplitude assumed to be very small compared to the background quantities $\chi_1/\chi_{eq} = \epsilon_d \ll 1$

Gyrokinetic equation in ORB5

- ORB5 (Lagrangian PIC) solves GK Vlasov-Maxwell system of equations
- Species distribution function f_s split between background $F_{0,s}$ and time dependent variation $f_s = F_{0,s} + \delta f_s$
- Background control variate $F_{0,s}$ chosen as Maxwellian
- Deviation δf_s found from GK Vlasov equation

$$\partial_t \delta f_s + \dot{R} \frac{\partial \delta f_s}{\delta R}\bigg|_{v_{||}} + \dot{v}_{||} \frac{\partial f_s}{\partial v_{||}} = -\dot{R}^{(1)} \cdot \frac{\partial F_{0,s}}{\partial R}\bigg|_{\varepsilon} - \dot{\varepsilon}^{(1)} \frac{\partial F_{0,s}}{\partial \varepsilon}$$

- Gyro-center orbits and trajectories $\left[\dot{R}, \dot{v}_{||}\right]$ with perturbations $\left[\dot{R}^{(1)}, \dot{v}_{||}{}^{1}\right]$
- Total energy $\varepsilon = \varepsilon_{||} + \varepsilon_{\perp} = \frac{1}{2} v_{||}^2 + \mu B$ with $\mu = \frac{v_{\perp}^2}{2B}$

▸ ORB5

Tearing Mode Initialisation in ORB5

- Unstable current profile (Wesson 11)
  $j = j_0 \left(1 - x^2\right)^{\zeta}$
  $q = q_a \frac{x^2}{1-(1-x^2)^{\zeta}+1}$
  $\zeta = 1,\ x = r/a$
- Shifted Maxwellian distribution for the electrons
- Mass ratio $m_i/m_e = 200$
- Large aspect ratio $R_0/a = 10$
  $\rho^* = \rho/a = 1/100$

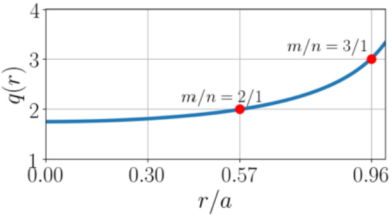

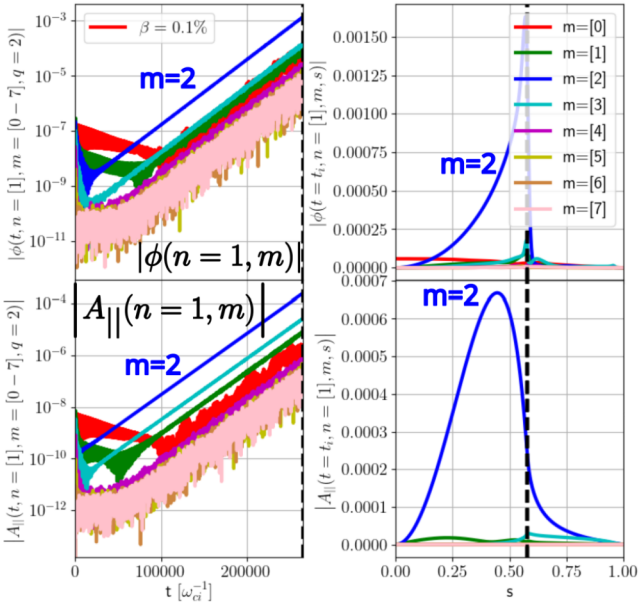

Codes Theory Benchmark I

Theoretical linear estimation of the growth rate using kinetic and two-fluids approach (Rogers et al., 2007)

$\gamma_{cl}/\gamma_{ci} = \Delta' \rho_{se} k_\theta \rho_{se} \left(\frac{m_e}{m_i}\right)^{1/2} \frac{1}{T_e^{1/2}} (T_e + T_i)^{1/2} \frac{1}{\beta_e}$ Validity: $m_e/m_i < \beta$

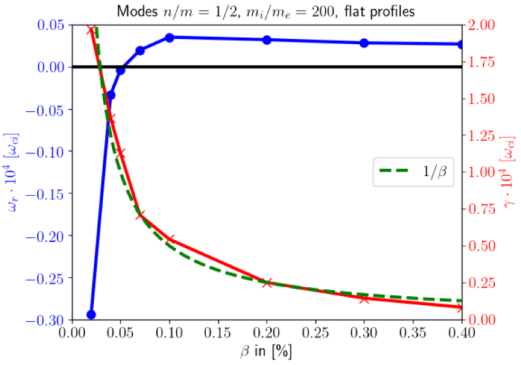

Widmer *et al.* 23 (in Prep)

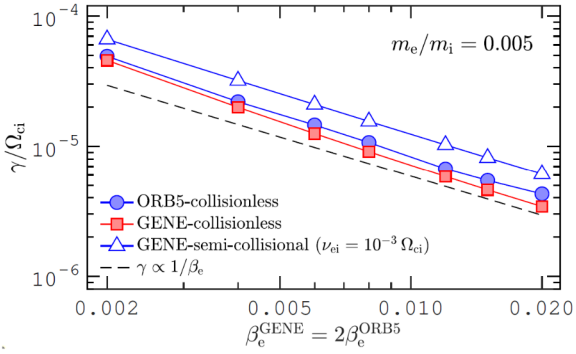

Jitsuk *et al.* 23 arXiv

Codes Theory Benchmark II

Theoretical linear estimation of the growth rate using kinetic and two-fluids approach (Rogers et al., 2007)

$\gamma_{cl}/\gamma_{ci} = \Delta' \rho_{se} k_\theta \rho_{se} \left(\frac{m_e}{m_i}\right)^{1/2} \frac{1}{T_e^{1/2}} (T_e + T_i)^{1/2} \frac{1}{\beta_e}$ Validity: $m_e/m_i < \beta$

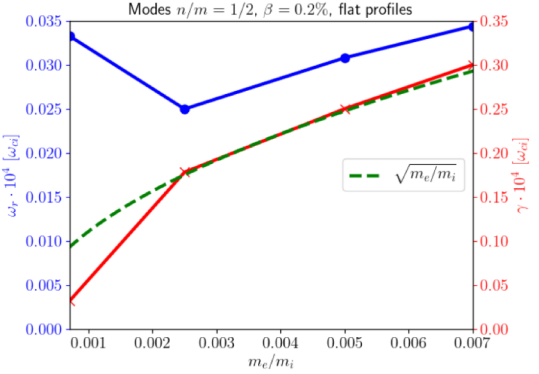

Widmer *et al.* 23 (in Prep)

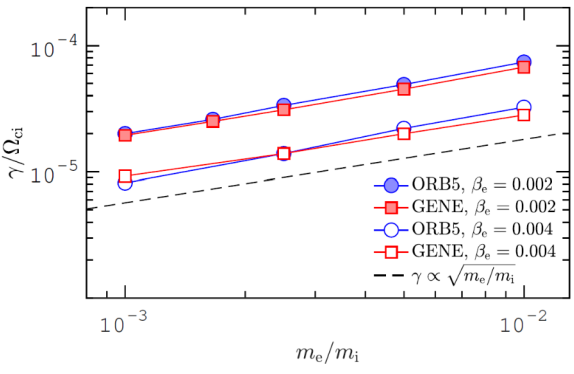

Jitsuk *et al.* 23 arXiv

CPUs Costs for Linear Runs

- Few markers are required since turbulence not present
- The electron skin depth $d_e = \sqrt{\frac{m_e}{m_i}\frac{1}{\beta}}\rho_s$ must be sufficiently resolved (radial direction)
- ORB5 grid resolution:
  - Radial grid s: depends on d_e
  - Poloidal χ and toroidal ϕ grid.
    Requirement: χ an integer multiple of ϕ and both must be integer multiples of the number of processes.
  - Toroidal resolution $\phi \gtrsim 4n_{max}$
  - Poloidal resolution $\chi \gtrsim 4(n_{max}q_{max} + \Delta m)$
  - Our simulations: $q_{max} = 3.25$ and $\Delta m = 5$

r/ρ_s	m_e/m_i	β	d_e/ρ_s	s	pts/d_e	n	ϕ	m	χ	Cpus/day	#Rsts
100	0.005	0.0005	3.2	307	9	1	8	7	48	384*24	1
100	0.000625	0.0005	1.11	907	9	1	8	7	48	384*24	4

Impact of Plasma–β and mass ratio, $\nabla T_s/T_s = \nabla n_s/n_s = 0$

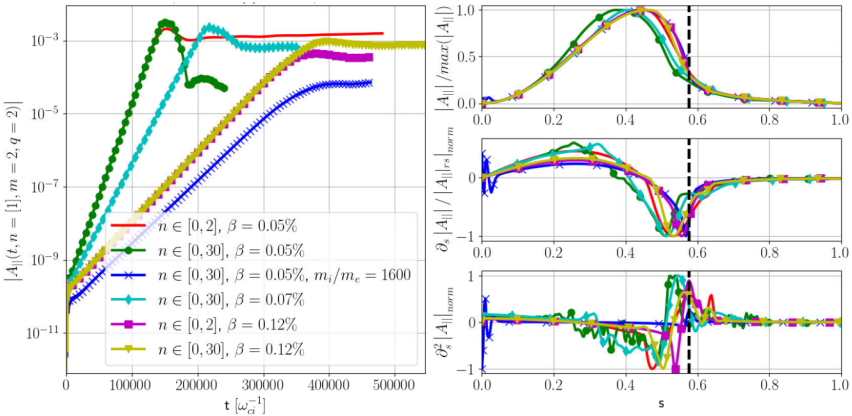

1. Skin depth must be resolved
2. Large n modes needed to include turbulence contribution to saturation
3. Small mass ratio results in strong growth and very large islands

r/ρ_s	m_e/m_i	β	d_e/ρ_s	s	pts/d_e	n	ϕ	m	χ	Cpus/day	#Rsts
100	0.005	0.0005	3.2	507	9	30	128	96	384	1536*24	20
100	0.000625	0.0005	1.11	907	9	30	128	96	384	1536*24	30

Toroidal Modes n spectrum, $\nabla T_s/T_s = \nabla n_s/n_s = 0$, $\beta_e = 0.05\%$

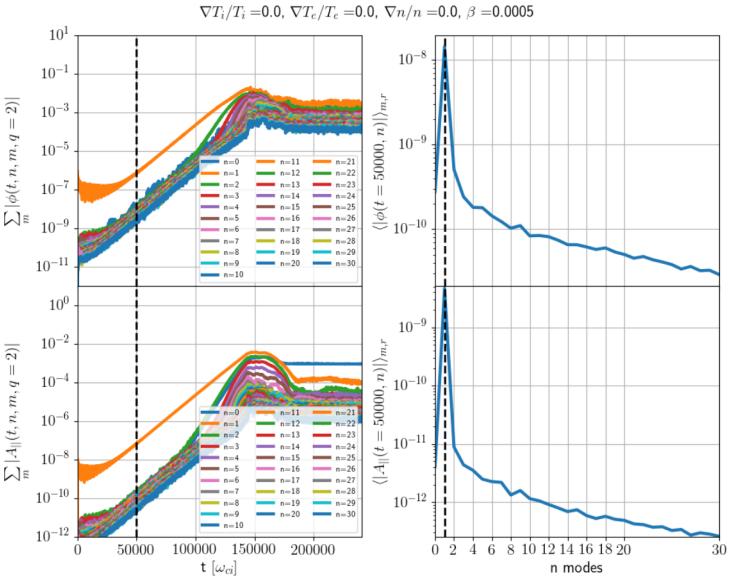

Helical Flux, $\nabla T_s/T_s = \nabla n_s/n_s = 0$, $\beta_e = 0.05\%$

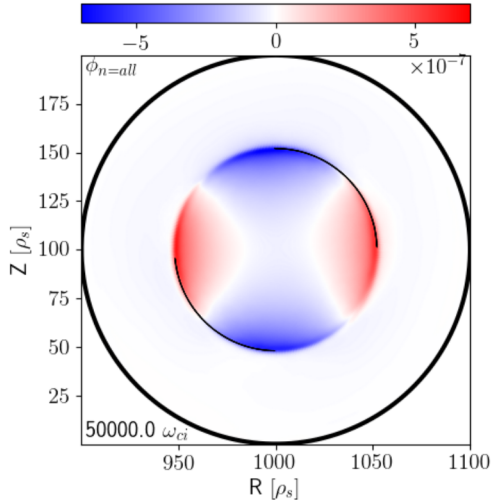

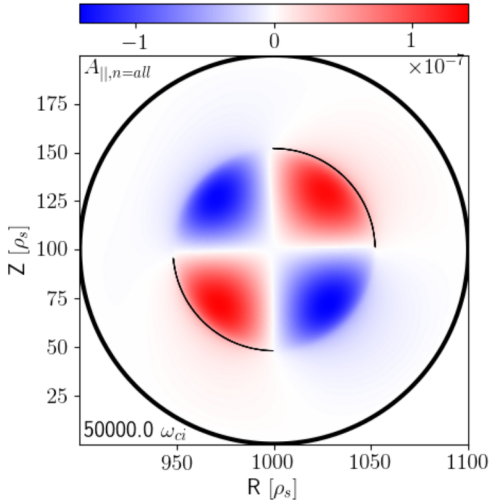

Island Overshoot

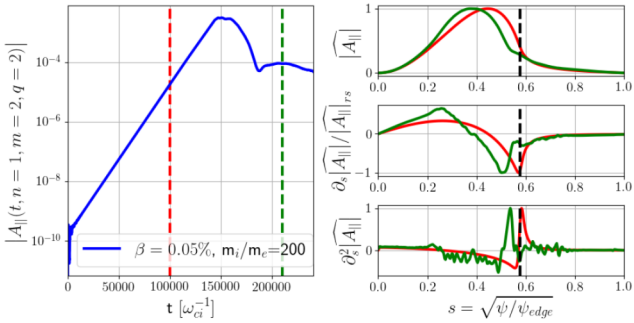

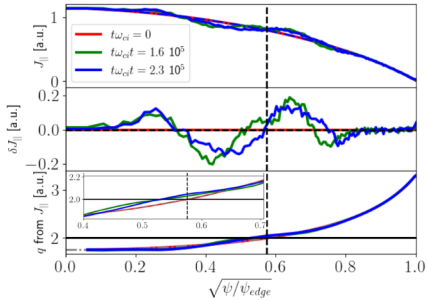

1. Heavy electrons result in strong growth and very large islands
2. The strong growth of the tearing leads to a large island
3. Turbulence due to local gradients at separatrix

Island poloidal Velocity

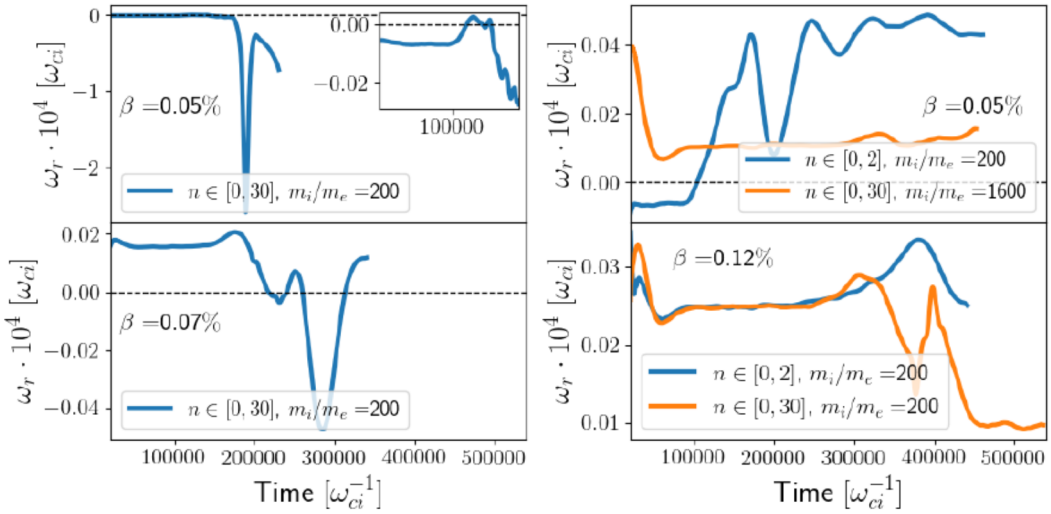

- Island poloidal velocity negligible except with overshoot

Zonal Flows

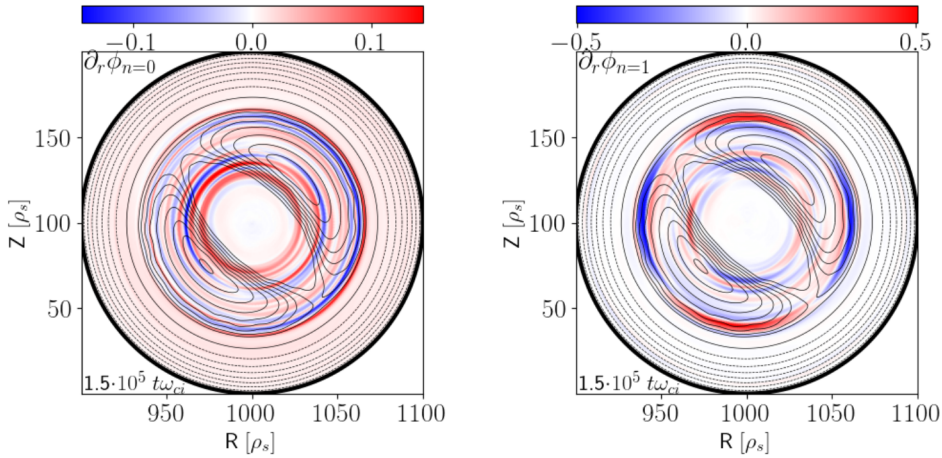

- The island generate a flow with helicity $m/n = 2/1$ to regulate the turbulence
- Island shrinks, zonal flows growth as electrostatic turbulence growth and contribute to island rotation direction

Summary

1. ORB5 can perform self consistent simulations of tearing mode and magnetic island growth. Successful benchmark with other GK codes.
2. Linear simulations relatively cheap
3. Non-linear simulations: the numerical cost could become large to properly resolve micro-instability and electron skin depth d_e
4. Several restarts generate a large amount of data that need to be stored
5. Mass ratio and plasma–β important: $d_e/\rho_s \propto \sqrt{\frac{m_e}{m_i}\frac{1}{\beta}}$
6. Large d_e results in large magnetic islands:
   1. Turbulence at sepratrix due to local gradients
   2. Current profile flattening and safety factor profile modified
   3. Strong acceleration of island poloidal rotation by zonal flows
7. Overshoot not realised at more realistic mass ratio or larger β.

B. N. Rogers, S. Kobayashi, P. Ricci, W. Dorland, J. Drake, and T. Tatsuno. Gyrokinetic simulations of collisionless magnetic reconnection. *Physics of Plasmas*, 14(9), 2007. ISSN 1070664X. doi: 10.1063/1.2774003.

Masaaki Yamada, Jongsoo Yoo, and Clayton E. Myers. Understanding the dynamics and energetics of magnetic reconnection in a laboratory plasma: Review of recent progress on selected fronts. *Physics of Plasmas*, 23(5):055402, may 2016. ISSN 1070-664X. doi: 10.1063/1.4948721. URL `http://dx.doi.org/10.1063/1.4948721http://aip.scitation.org/doi/10.1063/1.4948721`.

H P Furth, J Killen, M N Rosenbluth, Furth, Killeen, and Rosenbluth. FINITE-RESISTIVITY INSTABILITIES OF A SHEET PINCH. *Physics of Fluids*, 6(4):459–484, 1963.

F. Widmer, J. Büchner, and N. Yokoi. Characterizing plasmoid reconnection by turbulence dynamics. *Physics of Plasmas*, 23:092304, September 2016a. doi: 10.1063/1.4962694.

A. Bhattacharjee, Yi-Min Huang, H. Yang, and B. Rogers. Fast reconnection in high-Lundquist-number plasmas due to the plasmoid Instability. *Physics of Plasmas*, 16(11): 112102, November 2009. doi: 10.1063/1.3264103.

N.F. Loureiro, Alexander A. Schekochihin, and Steven Charles Cowley. Instability of current sheets and formation of plasmoid chains. *Physics of Plasmas*, 14:100703, 2007. doi: 10.1063/1.2783986.

A. Yoshizawa. Self-consistent turbulent dynamo modeling of reversed field pinches and planetary magnetic fields. *Physics of Fluids B*, 2:1589–1600, July 1990. doi: 10.1063/1.859484.

N. Yokoi and M. Hoshino. Flow-turbulence interaction in magnetic reconnection. *Physics of Plasmas*, 18(11):111208, November 2011. doi: 10.1063/1.3641968.

K. Higashimori, N. Yokoi, and M. Hoshino. Explosive Turbulent Magnetic Reconnection. *prl*, 110(25):255001, June 2013. doi: 10.1103/PhysRevLett.110.255001.

F. Widmer, J. Büchner, and N. Yokoi. Sub-grid-scale description of turbulent magnetic reconnection in magnetohydrodynamics. *Physics of Plasmas*, 23(4):042311, April 2016b. doi: 10.1063/1.4947211.

F. Widmer, J. Büchner, and N. Yokoi. Analysis of fast turbulent reconnection with self-consistent determination of turbulence timescale. *Physics of Plasmas*, 26(10):102112, October 2019a. doi: 10.1063/1.5109020.

A. Ishizawa, Y. Kishimoto, and Y. Nakamura. Multi-scale interactions between turbulence and magnetic islands and parity mixture—a review. *Plasma Physics and Controlled Fusion*, 61 (5):054006, May 2019. doi: 10.1088/1361-6587/ab06a8.

Fabien Widmer, Patrick Maget, Olivier Février, Hinrich Lütjens, and Xavier Garbet. Non-linear simulations of neoclassical tearing mode control by externally driven RF current and heating, with application to ITER. *Nuclear Fusion*, 59(10):106012, Oct 2019b. doi: 10.1088/1741-4326/ab300f.

Masaaki Yamada. Review of controlled laboratory experiments on physics of magnetic reconnection. *jgr*, 104(A7):14529–14542, July 1999. doi: 10.1029/1998JA900169.

Appendix

Magnetic Reconnection Globally Defined

- Plasma state: a highly conducting gas that composes 99% of the Universe visible matter
- Plasma generate magnetic fields $\boldsymbol{B}$ (dynamo)
- Magnetic reconnection: topological rearrangement of $\boldsymbol{B}$ because of connectivity change

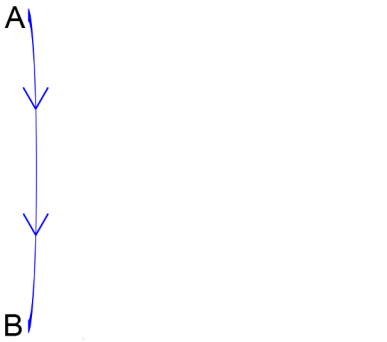

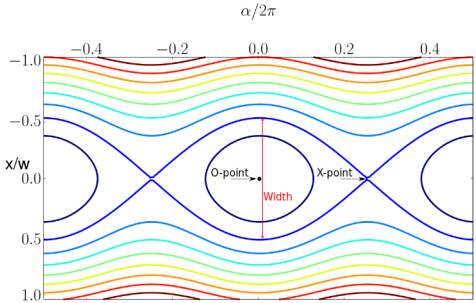

- Convert free $\boldsymbol{B}$ energy into other forms through unstable current sheet→ New equilibrium configuration with lower magnetic energy → particles heated and accelerated.

Ideal and single fluid resistive MHD

Plasma$\approx$ gas of charged particles reacting to electromagnetic fields.

Maxwell's Equations

- $\nabla \cdot \boldsymbol{E} = \rho/\epsilon_0$
- $\nabla \cdot \boldsymbol{B} = 0$
- $\nabla \times \boldsymbol{E} = -\partial_t \boldsymbol{B}$
- $\nabla \times \boldsymbol{B} = \mu_0 \boldsymbol{J}$

MHD

- $\frac{D\rho}{Dt} = 0$
- $\partial_t \boldsymbol{B} = -\nabla \times \boldsymbol{E}$
  - $\partial_t p + \boldsymbol{V} \cdot \nabla p + \gamma p \nabla \cdot \boldsymbol{V} = (\gamma - 1)\,\eta \boldsymbol{J}^2$
- $\frac{D\boldsymbol{V}}{Dt} = -\nabla p + \boldsymbol{J} \times \boldsymbol{B}$
- $\boldsymbol{E} = -\boldsymbol{V} \times \boldsymbol{B} + \eta \boldsymbol{J}$

- Ideal: $E_{||} = 0 \rightarrow$ magnetic field lines can never break or tear apart
- Resistive MHD dissipation mechanism through: $\eta = 4\pi\nu_{ei}/\omega_{pe}^2$

  $\omega_{pe} = e^2 n_e/(m_e \epsilon_0)$ electron plasma frequency

MHD Two-fluids

- Electrons and ions do not move as a single fluid in thin reconnection layer in collisionless plasmas.
- Two fluid dynamics: strong Hall current due to motion of magnetised electrons and demagnetized ions.
- Generalized Ohm's law

$$\boldsymbol{E} + \boldsymbol{V} \times \boldsymbol{B} = \eta \boldsymbol{J} + \frac{\boldsymbol{J} \times \boldsymbol{B}}{e n_e} - \frac{\nabla \cdot \boldsymbol{P}_e}{e n_e} - \frac{m_e}{e} \frac{d \boldsymbol{V}_e}{dt}$$

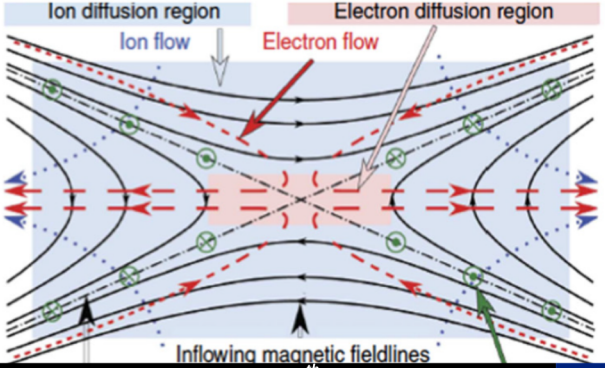

- $\boldsymbol{E} + \boldsymbol{V}_i \times \boldsymbol{B} \neq 0$
- $\boldsymbol{E} + \boldsymbol{V}_e \times \boldsymbol{B} = 0$
- $\boldsymbol{E} + \boldsymbol{V}_e \times \boldsymbol{B} \neq 0$
  - $E_{rec} \approx |\boldsymbol{V}_e \times \boldsymbol{B}_{rec}|$

$\Longleftarrow$ (Yamada et al., 2016)

Tearing mode I Furth et al. (1963)

Assume $\nabla \cdot \boldsymbol{V} = 0$, $\nabla \cdot \boldsymbol{B} \to \boldsymbol{k} \cdot \boldsymbol{B} = 0$ (instability along $\boldsymbol{B}$)

- $\boldsymbol{B}_0(x) = B_{0,y}(x)\boldsymbol{e}_y + \boldsymbol{B}_{0,z}(x)\boldsymbol{e}_z$
- $B_{0,y}(x) = \tanh(x/\delta)$
- $\boldsymbol{J}_{0,z}(x) = \partial_x \boldsymbol{B}_{0,z}(x)\boldsymbol{e}_z/\mu_0$
- $\boldsymbol{V} = \boldsymbol{e}_z \times \nabla\phi$ and $\boldsymbol{B} = \nabla A_z \times \boldsymbol{e}_z$

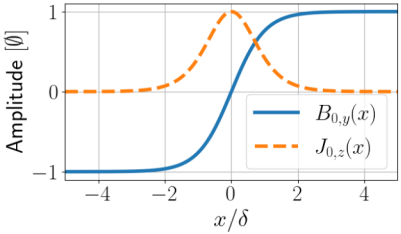

Take the $\boldsymbol{e}_z$ component of the pressure balance equation and Ampère's law together with induction equation

- Linear periodic perturbation in $\boldsymbol{e}_y$: $\widetilde{Q}(x,y,z) = \widetilde{Q}\exp(ik_y y - \omega t)$ with $\omega = \omega + i\gamma$
- $\rho\left(\partial_t + \boldsymbol{V}\cdot\nabla\right)\nabla_\perp^2\widetilde{\phi} = B_0^2\nabla_{||}\widetilde{J}_z$
- $\partial_t\widetilde{A}_z = \nabla_{||}\widetilde{\phi} - \eta\widetilde{J}_z$
- $\mu_0 J_z = \nabla_\perp^2\widetilde{A}_z$

Solution found by boundary-layer approach

Tearing Mode II

Outer layer

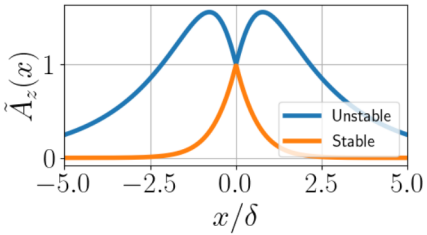

$$\widetilde{A}_z \propto e^{(-k_y|x|)}\left(1+\frac{\tanh(|x/\delta|)}{k_y\delta}\right)$$

- $\partial_x \widetilde{A}_z$ not continuous
- Tearing parameter $\Delta' = \lim_{\epsilon\to 0} \frac{\partial \ln(\tilde{A}_z)}{\partial x}\Big|_{x=-\epsilon}^{x=+\epsilon}$
- $\delta\Delta' = 2\left(\frac{1}{(\delta k_y)} - \delta k_y\right)$

Internal layer

- Linearised equations
- $-\rho\nabla_\perp^2\widetilde{\phi} = \nabla_{||}\widetilde{J}_z$
- $\widetilde{A}_z = -\nabla_{||}\widetilde{\phi} - \eta\widetilde{J}_z$
  $\hookrightarrow \gamma\widetilde{A}_z = \left(\frac{k_y^2 x^4}{\gamma\tau_A^2} + \frac{L_s^2}{\tau_R}\right)\frac{\partial^2\widetilde{A}_z}{\partial x^2}$
- Time scales:
  $\tau_R = \mu_0 L_s^2/\eta$
  $\tau_A = L_s(\mu_0\rho)^{1/2}/B_0$
- Shear length $L_s = B_0/B_{0,y}$

Tearing mode growth rate

$$\gamma = (\Delta')^{4/5} k_y^{2/5} L_s^{6/5} \tau_A^{-2/5} \tau_R^{-3/5} \approx \eta^{3/5}(\Delta')^{4/5}\left(\frac{k_y B_0}{L_s}\right)^{2/5}$$

MHD Secondary Tearing Instability (Plasmoid) (Loureiro et al., 2007)

SP CS (system size) unstable at sufficiently high $S=(L/\Delta)^2$ with $\gamma_{max} \approx S^{1/4} v_A / L_{CS}$

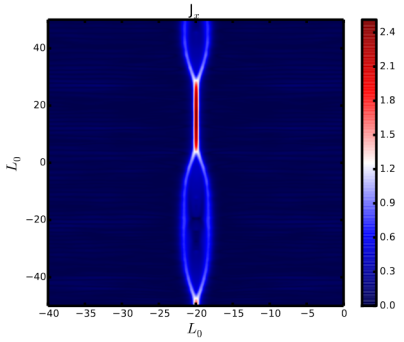

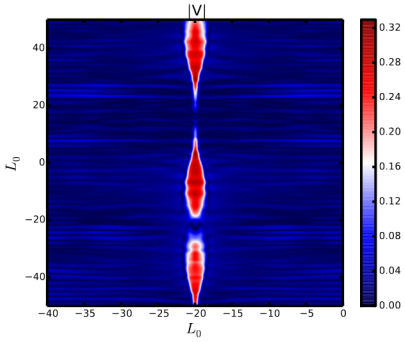

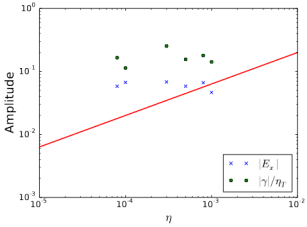

(Widmer et al., 2016a, Bhattacharjee et al., 2009)

Mean-Field Turbulence Model I: Mean-Field MHD

- Electromotive force (Yoshizawa, 1990) $\boldsymbol{\mathcal{E}} = \alpha\overline{\boldsymbol{B}} - \beta\overline{\boldsymbol{J}} + \gamma\overline{\boldsymbol{\Omega}}$ with $\overline{J} = \overline{\nabla \times \boldsymbol{B}}$ and $\overline{\Omega} = \overline{\nabla \times \boldsymbol{V}}$
- Mean induction equation

$$\partial_t \overline{\boldsymbol{B}} = -\nabla \times \left(\overline{\boldsymbol{E}} + \boldsymbol{\mathcal{E}}\right) = \nabla \times (\overline{\boldsymbol{V}} \times \overline{\boldsymbol{B}} + \gamma\overline{\boldsymbol{\Omega}} + \alpha\overline{\boldsymbol{B}}) - \nabla \times \left[(\beta + \eta)\overline{\boldsymbol{J}}\right]$$

Modelling (Yokoi and Hoshino, 2011)

$\alpha = C_\alpha \tau H$ by turbulent helicity: $H = \overline{-\boldsymbol{V}' \cdot \boldsymbol{\Omega}' + \boldsymbol{B}' \cdot \boldsymbol{J}'/\overline{\rho}}$

$\beta = C_\beta \tau K$ by turbulent energy: $K = \frac{1}{2}\overline{\boldsymbol{V}'^2 + \boldsymbol{B}'^2/(\mu_0\overline{\rho})}$

$\gamma = C_\gamma \tau W$ by turbulent cross-helicity: $W = \overline{\boldsymbol{V}' \cdot \boldsymbol{B}'/(\sqrt{\mu_0\overline{\rho}})}$

- Closure for K, W and H by evolution equations
- Turbulence timescale $\tau = \epsilon/K$

▸ EvoEQN

Mean-Feild Turbulence Model II: Turbulence Evolution Equations

Electromotive force model

$$\boldsymbol{\mathcal{E}} = \tau\left(-C_\beta K\overline{\boldsymbol{J}} + C_\gamma W\overline{\boldsymbol{\Omega}}\right)$$

$$\frac{\partial K}{\partial t} = -\overline{\boldsymbol{V}}\cdot\nabla K \overbrace{-\boldsymbol{\mathcal{E}}\cdot\overline{\boldsymbol{J}}}^{P_K} \overbrace{-\frac{K}{\tau}}^{\varepsilon_K} \overbrace{+\frac{\overline{\boldsymbol{B}}}{\sqrt{\overline{\rho}}}\cdot\nabla W}^{T_K}$$

$$\frac{\partial W}{\partial t} = -\overline{\boldsymbol{V}}\cdot\nabla W \underbrace{-\boldsymbol{\mathcal{E}}\cdot\overline{\boldsymbol{\Omega}}}_{P_W} \underbrace{-C_W\frac{W}{\tau}}_{\varepsilon_W} \underbrace{+\frac{\overline{\boldsymbol{B}}}{\sqrt{\overline{\rho}}}\cdot\nabla K}_{T_W}$$

Production terms: P_K and P_W

Dissipation terms: ε_κ and ε_w

Transport terms: T_K and T_W

◂ $\alpha\beta\gamma$

Mean-Field Turbulence Model III: Simulation results

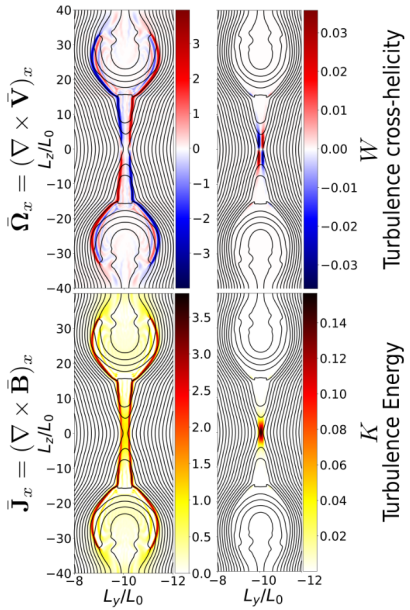

- Turbulence enhances reconnection (τ dependence) by anomalous resistivity (Higashimori et al., 2013, Widmer et al., 2016b)
- Turbulence always enhances reconnection (in this model) (Widmer et al., 2019a)

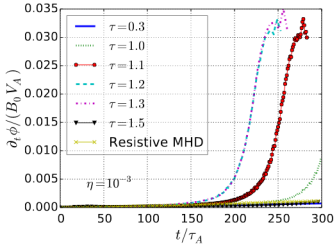

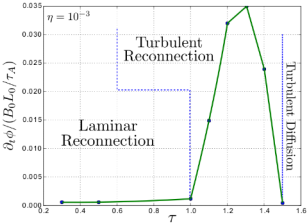

Procedure

1. Solve MHD equations

$$\begin{aligned}
\frac{\partial \overline{\rho}}{\partial t} &= -\nabla \cdot (\overline{\rho}\boldsymbol{V}) \\
\frac{\partial \overline{\rho}\boldsymbol{V}}{\partial t} &= -\nabla \cdot \left[\overline{\rho}\boldsymbol{V} \otimes \boldsymbol{V} + \frac{1}{2}\left(p + B^2\right)\boldsymbol{I} - \boldsymbol{B} \otimes \boldsymbol{B}\right] + \chi \nabla^2 (\overline{\rho}\boldsymbol{V}) \\
\frac{\partial \boldsymbol{B}}{\partial t} &= \nabla \times (\boldsymbol{V} \times \boldsymbol{B}) + \eta \nabla^2 \boldsymbol{B} \\
\frac{\partial h}{\partial t} &= -\nabla \cdot (h\boldsymbol{V}) + \frac{\gamma_0 - 1}{\gamma_0 h^{\gamma_0 - 1}}\left(\eta \boldsymbol{J}^2\right) + \chi \nabla^2 h
\end{aligned}$$

2. Compute turbulence by mean of a Gaussian filter

$$\begin{aligned}
\overline{K} &= \frac{1}{2}\left[\left(\overline{\boldsymbol{V}^2} - \overline{\boldsymbol{V}}^2\right) + \left(\overline{\boldsymbol{B}^2} - \overline{\boldsymbol{B}}^2\right)/(\mu_0 \overline{\rho})\right] \\
\overline{W} &= \left(\overline{\boldsymbol{V} \cdot \boldsymbol{B}} - \overline{\boldsymbol{V}} \cdot \overline{\boldsymbol{B}}\right)/(\sqrt{\mu_0 \overline{\rho}}) \\
\overline{H} &= -\left(\overline{\boldsymbol{V} \cdot \boldsymbol{\Omega}} - \overline{\boldsymbol{V}} \cdot \overline{\boldsymbol{\Omega}}\right) + \left(\frac{\overline{\boldsymbol{B} \cdot \boldsymbol{J}} - \overline{\boldsymbol{B}} \cdot \overline{\boldsymbol{J}}}{\overline{\rho}}\right)
\end{aligned}$$

Gyrokinetic equation in ORB5 II

- Mixed variable formalism: $A_{||} = A^h_{||} + A^s_{||}$
- Gyrocenter orbits equations for $\dot{R} = \dot{R}^{(0)} + \dot{R}^{(1)}$ and $\dot{v}_{||} = \dot{v}_{||}{}^{(0)} + \dot{v}_{||}{}^{(1)}$
- Unperturbed $\dot{R}^{(0)} = v^{(0)}_{||}\boldsymbol{b_0}^* + \frac{1}{qB^*_{||}}\boldsymbol{b} \times \mu\nabla B$ and $\dot{v}^{(0)}_{||} = -\frac{\mu}{m}\boldsymbol{b_0}^* \cdot \nabla B$
- Perturbed

$$\begin{aligned} \dot{R}^{(1)} &= \frac{\boldsymbol{b}}{B^*_{||}} \times \nabla\langle\phi - v_{||}A_{||}\rangle - \frac{q}{m}\langle A^{(h)}_{||}\rangle\boldsymbol{b_0}^* \\ \dot{v}_{||}{}^{(1)} &= \frac{-q}{m}\left[\boldsymbol{b_0}^* \cdot \nabla\langle\phi - v_{||}A^h_{||} + \partial_t A^s_{||}\rangle\right] - \frac{\mu}{m}\frac{\boldsymbol{b}\times\nabla B}{B^*_{||}} \cdot \langle A^s_{||}\rangle \end{aligned} \quad (1)$$

- $\boldsymbol{b}^* = \boldsymbol{b_0}^* + \frac{\langle A^s_{||}\rangle \times \boldsymbol{b}}{B^*_{||}}$, $\boldsymbol{b_0}^* = \boldsymbol{b} + \frac{mv_{||}}{qB^*_{||}}\nabla \times \boldsymbol{b}$, $B^*_{||} = B + \frac{mv_{||}}{q}\boldsymbol{b} \cdot \nabla \times \boldsymbol{b}$; $b = B/|B|$
- Quasi-neutrality: $-\nabla \cdot \left(\frac{n_0}{B\omega_{ei}}\nabla_\perp\phi\right) = \bar{n}_{1,i} - \bar{n}_{1,e}$
- Ampère's law: $\sum_s \frac{\beta_s}{\rho_s^2}A^h_{||} - \nabla^2_\perp A^h_{||} = \mu_0 \sum_s \bar{j}_{||,1,s} + \nabla^2_\perp A^s_{||}$

▸ ORB5

Tokamak Purpose and Goals

- Obtain a continuous large amount of energy at minimal risks (environment, radioactivity, chain reactions)
- Fusion of hydrogen isotopes: Deuterium (D) and Tritium (T) to form heavier nucleus $^2\mathrm{D} + {}^3\mathrm{T} \rightarrow {}^4\mathrm{He}\ (E_\alpha = 3.5\mathrm{MeV}) + {}^1\mathrm{n}\ (E_n = 14.1\mathrm{Mev})$
- Bring the matter to a plasma state by heating to several keV$\cong 10^8$K
- Confine the plasma expansion due to heating by strong magnetic field

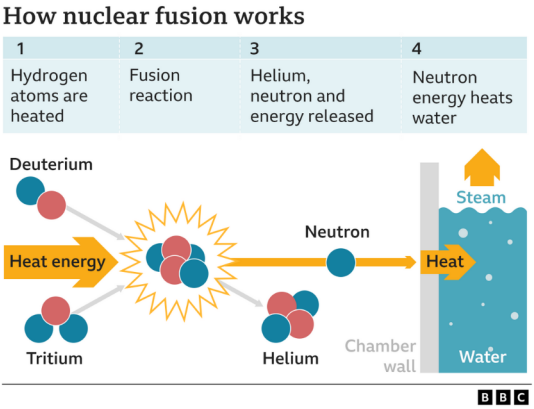

Slab

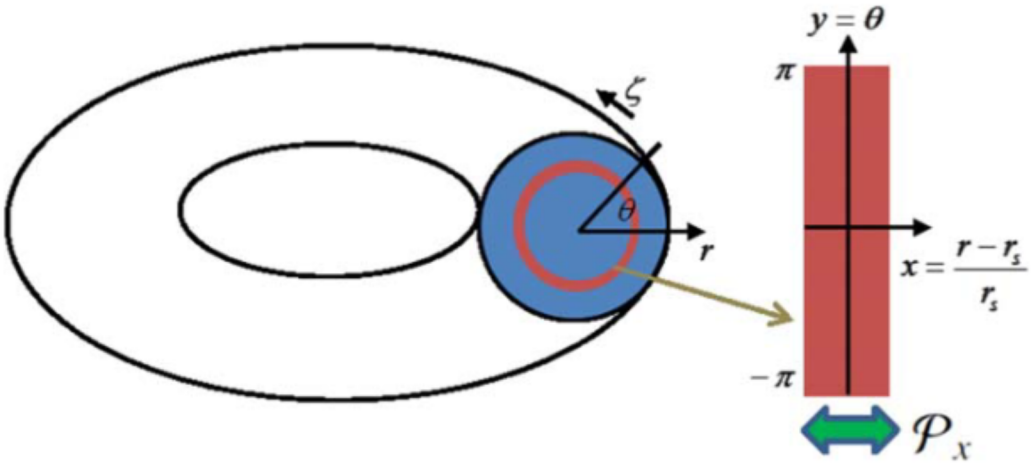

Figure 5. Parity operator $\mathcal{P}_x$ in the radial direction.

Figure – Schematic view of slab Ishizawa et al. (2019)

Tokamak Design and Operation

Axisymmetric torus-shaped vessel with large magnetic field, moderate plasma pressure and small toroidal current.

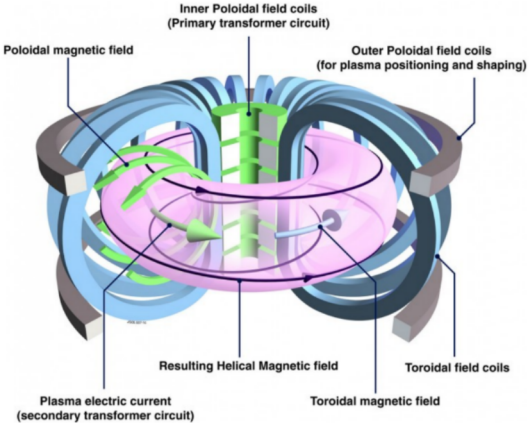

Figure – Schematic view of a Tokamaks www.ccfe.ac.uk. Drifts

1. A large toroidal magnetic field $\boldsymbol{B}_\varphi$ is generated by the outer toroidal field coils (blue). This fields generates particle drifts in the vertical direction.
2. Injection of (often pre-ionised) neutral gas in the vacuum chamber.
3. Toroidal plasma current induced by the transformer, ramped up to its maximum. Poloidal magnetic field $\boldsymbol{B}_\theta$ is generated, counter-acting the drifts. $\boldsymbol{B} = \boldsymbol{B}_\varphi + \boldsymbol{B}_\theta$
4. External RF or neutral beam heating applied to the plasma.

Tokamak Equilibrium State I: MHD equations

- Static state: $\rightarrow \partial_t \boldsymbol{B} = \partial_t p = \partial_t \rho = \partial_t \boldsymbol{V} = 0$
- MHD equation for plasma at rest

$$\begin{aligned} \boldsymbol{J} \times \boldsymbol{B} &= \nabla p, & (2)\\ \boldsymbol{J} &= \nabla \times \boldsymbol{B}, & (3)\\ \nabla \cdot \boldsymbol{B} &= 0, & (4) \end{aligned}$$

- Satisfying eq.(2) implies

$$\boldsymbol{B} \cdot \nabla p = 0, \quad \boldsymbol{J} \cdot \nabla p = 0. \qquad (5)$$

$\boldsymbol{B}$ and $\boldsymbol{J}$ span magnetic surfaces that are also surfaces of constant pressure on which particle are confined.

Tokamak Equilibrium State II: Flux surfaces label

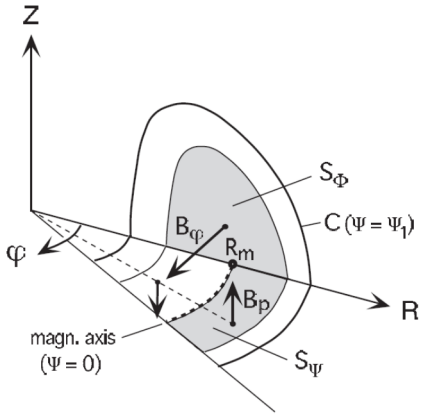

- Magnetic surfaces: continuous sequence of magnetic toroids nested around a single closed curve named magnetic axis ($\Psi = 0$)
- Magnetic surface label Ψ

$$\Psi \equiv \frac{1}{2\pi} \int B_\theta \, dS_\Psi . \tag{6}$$

Tokamak Geometrical Aspects III: Safety factor q

- Safety factor q: parameter measuring the magnetic field line twist.
- q labels the flux surfaces defining their helicity.
- Poloidal angle θ defined such that $q = q(r)$

$$q(r) = \frac{\boldsymbol{B} \cdot \nabla \varphi}{\boldsymbol{B} \cdot \nabla \theta}. \tag{7}$$

- The safety factor represents the progression of the field line over the toroidal angle after one full poloidal revolution.

TCV Tokamak #64680 Experimental Profiles I

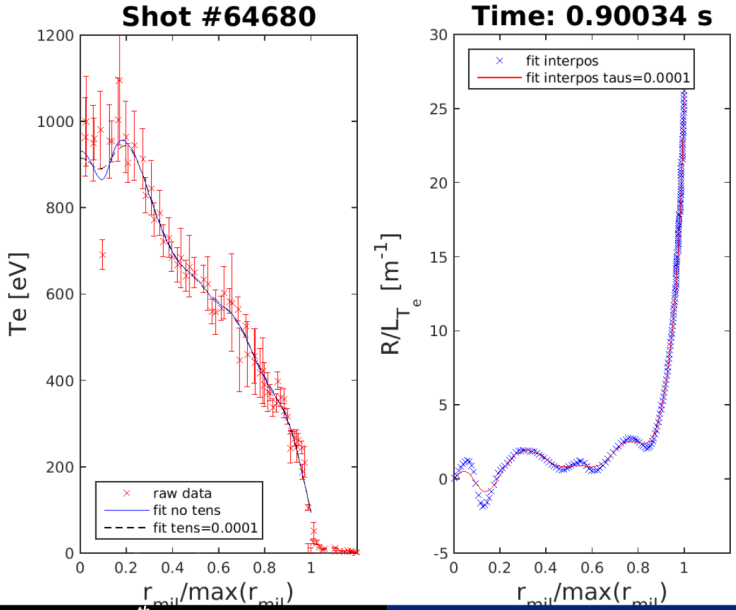

TCV Tokamak #64680 Experimental Profiles II

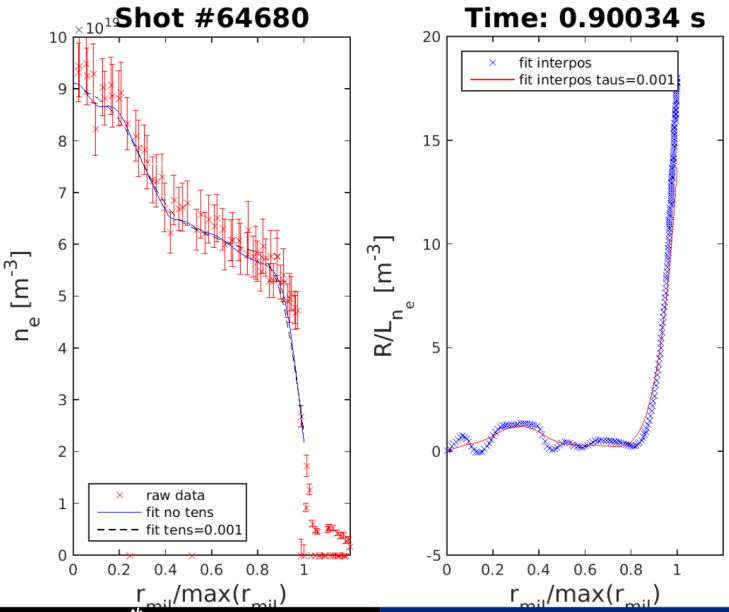

Bound to Magnetic Field lines (low collisionality)

- Motion in homogeneous and uniform $\boldsymbol{B}$

$$m_s \frac{d\boldsymbol{v}}{dt} = \boldsymbol{F} + Z_s e \boldsymbol{v} \times \boldsymbol{B}$$

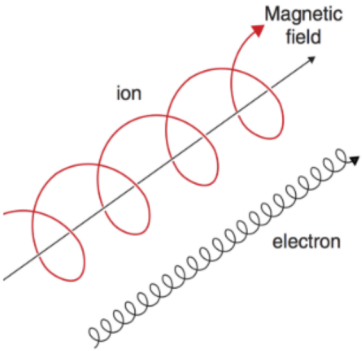

- Case of $\boldsymbol{F} \cdot \boldsymbol{B} = 0$
- Stream along $\boldsymbol{B}$ at $\boldsymbol{v}_{||}$ =cst.
- Parallel velocity $v_\perp = |\boldsymbol{v} \times \boldsymbol{B}|/B \cong v_{th} = \sqrt{2T_s/m_s}$

- Rapid Gyration around $\boldsymbol{B}$ with gyro-frequency Ω_{cs} and -radius ρ_s

$$\Omega_{cs} = \frac{Z_s e B}{m_s} \tag{8}$$

$$\rho_{cs} = \frac{v_\perp}{\Omega_{cs}} = \frac{m_s v_\perp}{Z_s e B} \tag{9}$$

- Ω_{cs} and ρ_s spatial and time scales in Tokamaks

Particle Drifts

- Motion in homogeneous and uniform $\boldsymbol{B}$

$$m_s \frac{d\boldsymbol{v}}{dt} = \boldsymbol{F} + Z_s e \boldsymbol{v} \times \boldsymbol{B} \tag{10}$$

- Case of $\boldsymbol{F} \cdot \boldsymbol{B} \neq 0$
- Solve eq.(10) with adiabatic theory: $|\partial_t \ln [\boldsymbol{B}, \boldsymbol{E}]| \ll \Omega_{cs}$ and $\rho_{cs} \left| \frac{\nabla B}{B} \right| \ll 1$.
- Drifts $\boldsymbol{v}_D = \boldsymbol{F} \times \boldsymbol{B}/(eB)$
- Prominent drifts in tokamak: ∇B, curvature κ and $\boldsymbol{E} \times \boldsymbol{B}$

$$v_D = \frac{1}{Z_s e} \left[\frac{m_s v_{||,s}^2}{B} + \underbrace{\frac{m_s v_{\perp,s}^2}{2B}}_{\mu} \right] \frac{\boldsymbol{B} \times \nabla B}{B^2} + \frac{\boldsymbol{E} \times \boldsymbol{B}}{B^2} \tag{11}$$

TokDes

Banana Orbits

- Conservations of μ and kinetic energy $\epsilon = \frac{mv_{||}^2}{2} + \mu B_0$ implies

$$\mu = \frac{\epsilon - mv_{||}^2/2}{B_0} \propto R\left(\epsilon - \frac{mv_{||}^2}{2}\right) \tag{12}$$

- Possibility of $\boldsymbol{v}_{||} = 0$ at HFS if $\boldsymbol{v}_{||} \ll \boldsymbol{v}_{\perp}$
  $\Rightarrow$ Particle is trapped, bouncing between HFS and LFS and drifting
  $\rightarrow$ **Banana orbits**

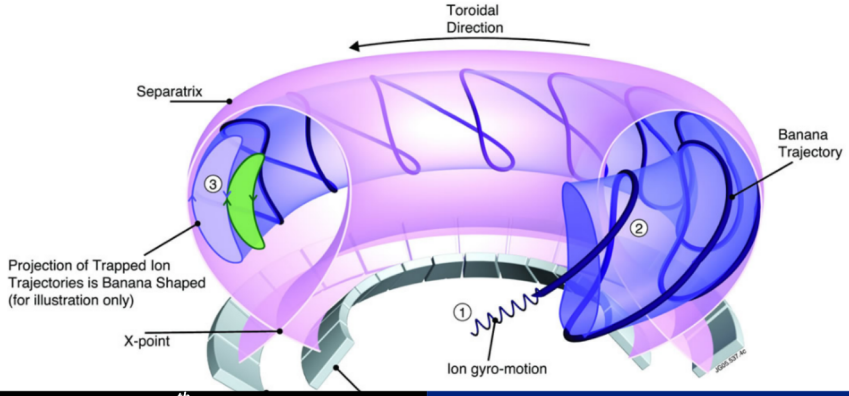

2D Magnetic Reconnection

- Magnetic reconnection: modification of magnetic field topology leading to the formation of island-shaped magnetic structures.

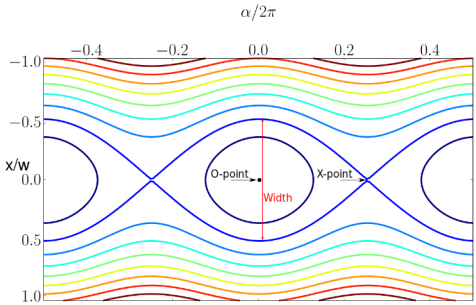

- Island : Width $w(r)$, center 'O'-point, diffusion region 'X'-point
- Island location: rational surfaces $q = m/n$
- Island wind around the tokamak helically with the same helicity ($q = m/n$) as the rational surface where they appear
- Wave length set by toroidal geometry

Island impact on Tokamak confinement

- Island toroidal and poloidal periodicity in expressed by Fourier modes (n, m)
- Fast parallel transport of heat flattens pressure (p) profiles inside the island
- Fusion device performance reduction related to, $w(r)$, ω_{isl}, q_O and spatial distribution.

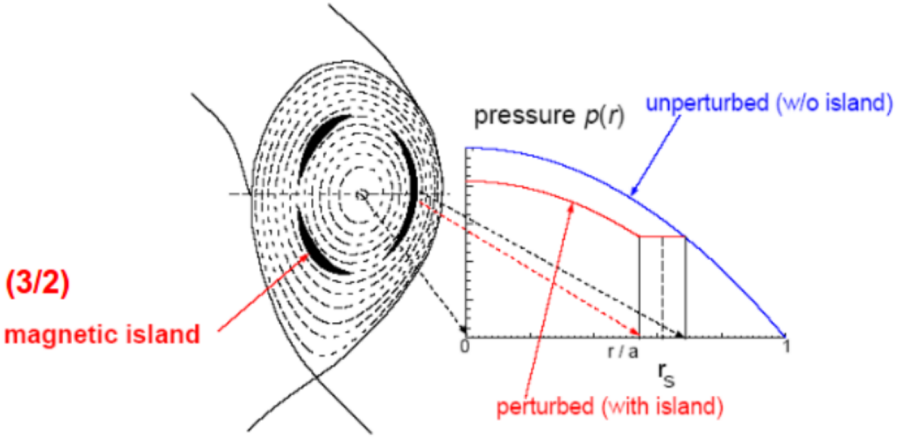

Neo-Classical-Tearing (NTM) Modes II

- NTM disappear if $W = w/a < w_{crit}$
- NTM non-linear evolution for ITER parameters by the Generalized Rutherford Equation (Widmer et al., 2019b)

$$\frac{0.82\mu_0 a^2}{\eta}\frac{dW}{dt} = a\Delta' + a\Delta'_{bs} + a\Delta'_{GJJ} + a\Delta'_{ctrl} + \dots$$

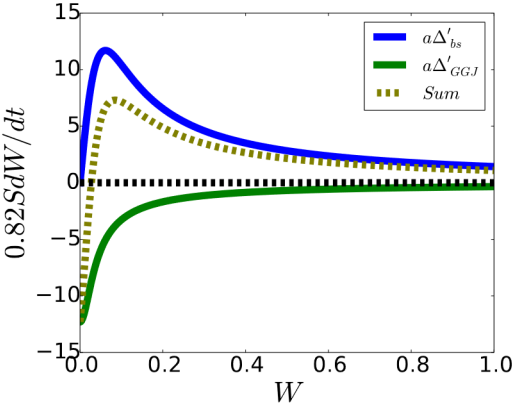

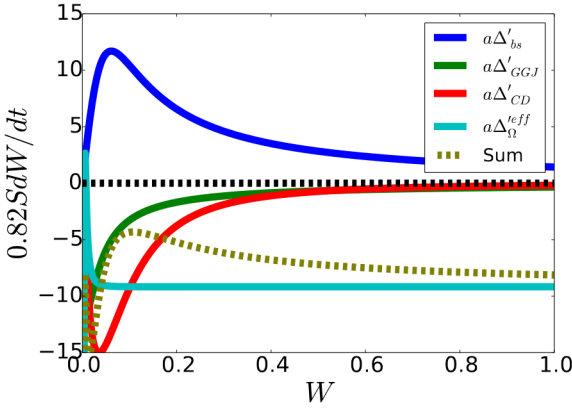

Laboratory: The Magnetic Reconnection Experiment (MRX) https://mrx.pppl.gov/

Dedicated experiment to study magnetic reconnection

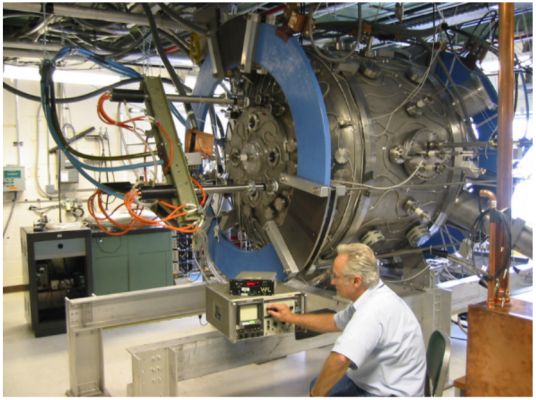

The vacuum vessel and equilibrium field coils (blue) of MRX

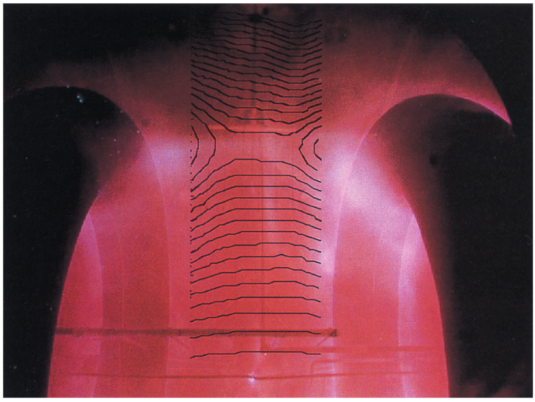

A plasma discharge in MRX. The two flux cores and magnetic diagnostics are visible.

Contours of constant fluxes are determined by experimental data of 30 magnetic probes (Yamada (1999))

Time scales in plasmas

- Resistive time $\tau_R = \mu_0 L^2/\eta$
  - Solar corona:
  - Fusion: $\tau_R \cong 6.4$s for $T_e = 1$keV and $n_e = 10^{14}\text{cm}^{-3}$
- Ideal MHD (Alfvén time) $\tau_A = L/\boldsymbol{V}_A$
  - Solar corona: τ_A
  - Fusion: $\tau_R \cong 1.1 \cdot 10^{-7}$s for $T_e = 1$keV and $n_e = 10^{14}\text{cm}^{-3}$